Tellus SERIES B CHEMICAL AND PHYSICAL METEOROLOGY
PUBLISHED BY THE INTERNATIONAL METEOROLOGICAL INSTITUTE IN STOCKHOLM

Relationship between fine-mode AOD and precipitation on seasonal and interannual time scales

By HWAYOUNG JEOUNG[1], CHUL E. CHUNG[1]*, TWAN VAN NOIJE[2] and TOSHIHIKO TAKEMURA[3], [1]*School of Environmental Science and Engineering, Gwangju Institute of Science and Technology, Gwangju 500-712, Korea;* [2]*Royal Netherlands Meteorological Institute, De Bilt, The Netherlands;* [3]*Research Institute for Applied Mechanics, Kyushu University, Fukuoka, Japan*

(Manuscript received 10 October 2013; in final form 11 December 2013)

ABSTRACT

On seasonal and interannual time scales, weather is highly influential in aerosol variability. In this study, we investigate the relationship between fine-mode AOD (fAOD) and precipitation on these scales, in order to unravel the effect of wet weather on aerosol amount. We find with integrated satellite and ground observations that biomass burning related fAOD has a relatively greater seasonal variation than fossil fuel combustion related fAOD. It is also found that wet weather reduces biomass burning fAOD and increases fossil fuel combustion fAOD. Aerosol simulation models forced by reanalyses consistently simulate the biomass burning fAOD reduced during wet weather but only in the tropics and furthermore do not consistently increase fossil fuel combustion fAOD during wet conditions. The identified relationship between fAOD and precipitation in observations allows for seasonal predictability of fAOD, since average precipitation can be predicted a few to several months in advance due to the well-established predictability of El Niño-Southern Oscillation (ENSO). We reveal ENSO-covariant fAOD using a rotated component principal analysis of combined interannual variation of sea surface temperature, precipitation and fAOD. During the warm phase of ENSO, we find that fAOD increases over Indonesia and the eastern coastal area of China, and decreases over South Asia, the Amazon and the continental parts of China.

Keywords: aerosol, AOD, aerosol simulation, weather, meteorology, prediction

1. Introduction

The amount, distribution and composition of aerosols in the atmosphere are controlled by emission and weather. Weather affects aerosols by various meteorological variables such as temperature, humidity, cloud cover, precipitation, wind and boundary layer stability. Jacob and Winner (2009) summarised how each meteorological variable influences aerosol dry mass in aerosol simulations. For example, higher humidity causes greater aerosol mass, while precipitation decreases aerosol mass. Tai et al. (2010), by analysing PM2.5 observations, showed that humidity, with other meteorological variables held fixed, is positively correlated with sulphate and nitrate, but negatively with organic aerosol (OA) and black carbon (BC). Note that meteorological variables are consistent with one another dynamically, thermodynamically and physically. For instance, precipitation tends to be accompanied by high moisture and larger cloud coverage.

On multidecadal to centurial time scales, anthropogenic aerosol emission can change several-fold (Lamarque et al., 2010), and so emission can be the driving factor in determining aerosols. On the other hand, on seasonal and interannual (2 ~4 years) scales, weather is expected to be a relatively more important factor in determining the variability of aerosols. On these time scales, aerosol emissions resulting from fossil fuel combustion fluctuate noticeably but much less than several-fold in most places. For instance, SO_2 emission in China is estimated to vary 20% seasonally and 30–40% interannually (Lu et al., 2011). SO_2 emission is a good proxy for fossil fuel combustion. Emission of biomass burning aerosols is estimated to vary noticeably too (Van der Werf et al., 2006; Cohen and Wang, 2013). For instance, over open biomass burning regions in Africa, the emission was estimated to change from year-to-year by about 15–20% (Van der Werf et al., 2006; Cohen and Wang, 2013). This fluctuation of biomass

*Corresponding author.
email: eddy@gist.ac.kr

Citation: Tellus B 2014, **66**, 23037, http://dx.doi.org/10.3402/tellusb.v66.23037

burning aerosol emission appears to be largely weather related. Murdiyarso and Adiningsih (2007) explain that dry weather conditions are more suitable for biomass burning. Weather can also account, at least partially, for seasonal or interannual fluctuations of fossil fuel combustion though the extent is not known. Overall, it is safe to say that weather is highly influential in aerosol variability on seasonal and interannual scales. We also note that volcanic eruptions can disturb the aerosol amount and characteristics greatly for up to 2 years, and volcanic eruptions are considered weather independent.

In the present study, we attempt to unravel the relationships between aerosol and precipitation on seasonal and interannual time scales. Correlations between PM concentration and meteorological variables have been investigated in the past (Koch et al., 2003; Wise and Comrie, 2005; Tai et al., 2010). When precipitation occurs, it scavenges aerosols and removes them from the atmosphere. The accompanying cloudiness decreases the photochemical oxidation of SO_2 and decreases sulphate, while in-cloud production increases sulphate (Jacob and Winner, 2009). The accompanying moisture enlarges sulphate aerosol by water uptake (Hess et al., 1998). The wet condition associated with precipitation would suppress open biomass burning. We include all these effects by seeking a simple correlation or covariance of aerosol and precipitation. A unique aspect of our study is that we seek to explore seasonal (a few to several months) predictability of aerosols. Precipitation has short-term climate predictability given the influence of El Niño-Southern Oscillation (ENSO). ENSO is being successfully predicted several months in advance (e.g. US Climate Prediction Center). Ropelewski and Halpert (1987) demonstrated that during El Niño phase precipitation decreases over Indonesia and Australia while precipitation is enhanced over the southern portion of the US. Precipitation predictability can lead to aerosol predictability, once a precipitation–aerosol relationship is established. Studies addressing ENSO impacts on aerosols exist; for instance, Wu et al. (2013) revealed a biennial component of aerosol variability over the Maritime Continent (5°S–5°N, 95–135°E) and the western North Pacific Ocean. The novelty of the current study is to analyse the fine-mode aerosol optical depth (fAOD) in relation to ENSO.

Aerosols have different sizes, and typically follow a bimodal structure in terms of fine mode and coarse mode (Kim et al., 2007; Viskari et al., 2012). Fine-mode aerosols usually have submicron sizes in diameter and consist largely of BC, OA, sulphate, or nitrate. These small particles are mostly anthropogenic. Schwartz and Neas (2000) reported that small particles are more harmful for human respiratory health than coarse-sized particles. One can use PM1.0 measurements to study fine-mode particles. Here, we focus on fAOD because optical depth carries additional useful information such as visibility and the impact on the radiation balance. We analyse fAOD also because satellite measurements give a nearly global coverage. Global AOD (aerosol optical depth) can be obtained from the Moderate Resolution Imaging Spectroradiometer (MODIS) and Multi-angle Imaging Spectroradiometer (MISR) satellite sensors. The fine-mode fraction (FMF) of total AOD is also retrieved and its retrieval algorithm depends heavily on the spectral variation of AOD (Remer et al., 2005). Due to the uncertainties in the spectral variation of land surface albedo, satellite-derived FMF is not reliable over land. Lee and Chung (2013) on the other hand constructed more reliable FMF over the globe by nudging satellite data towards Aerosol Robotic NETwork (AERONET) data. We will analyse fAOD data from Lee and Chung (2013). For comparison, global aerosol simulations will also be analysed.

Aerosols also affect weather and climate. Aerosols scatter and absorb solar radiation in the atmosphere (the so-called direct effect). Big particles such as dust and sea salt also absorb longwave radiation. The absorption of radiation increases air temperature. The absorption and scattering of radiation reduces the radiation reaching the surface and will likely decrease evaporation and precipitation (Ramanathan et al., 2001). Some of the aerosols can absorb sunlight efficiently and heat the atmosphere. This heating can evaporate cloud condensate and reduce cloud amount (the so-called semi-direct effect). Some aerosols act as cloud condensation nuclei (CCN), thus affecting cloud albedo and lifetime (the so-called indirect effect). By seeking the relationships between aerosol and precipitation, we do not separate the effect of meteorology on aerosol from that of aerosol on weather. Such separation is very important to validate models but irrelevant to empirical prediction of aerosol based on correlation between precipitation and aerosol.

We organise the paper in six sections. Section 2 describes the observations and model simulations. In section 3, we discuss the climatology and variance of fAOD. The correlation between precipitation and fAOD is discussed in section 4. In section 5, we describe ENSO-covariant fAOD. Conclusion and discussion follow in section 6.

2. Data

In this section, we describe the observations and model simulations employed for the analysis here. All the data (including simulation results) are monthly means and processed onto the T42 spatial resolution before statistical analyses. The T42 resolution is approximately $2.8^\circ \times 2.8^\circ$.

2.1. Observation

AOD and fAOD are obtained by the approach described in Lee and Chung (2013), who integrated monthly mean MODIS, MISR and AERONET data. They integrated these data by nudging the combined satellite data towards the AERONET data so as to construct reliable AOD and fAOD fields over the globe. We refer to this integrated data as MODIS + MISR + AERONET data here. As Lee and Chung (2013) explain, the data integration consists of the following steps: (1) MODIS and MISR data are combined to reduce the data gaps and improve the accuracy; (2) the remaining gaps are filled by the Georgia Tech/Goddard Global Ozone Chemistry Aerosol Radiation and Transport (GOCART) simulation (Chin et al., 2002); and (3) the combined MODIS + MISR + GOCART data are nudged towards the AERONET data as though the MODIS + MISR + GOCART data were an interpolation tool. The GOCART simulations in the MODIS + MISR + GOCART data are predominantly confined to the polar regions.

Lee and Chung (2013) also validated the MODIS + MISR + AERONET fAOD and found that this fAOD is closer to AERONET fAOD accuracy than MODIS or MISR fAOD accuracy. The MODIS + MISR + AERONET AOD and fAOD data span from 2001 to 2010. To facilitate the data comparison, we also analyse 2001–2010 MODIS AOD, which has gaps.

Precipitation data is taken from the Global Precipitation Climatology Project (GPCP) (Adler et al., 2003). The sea surface temperature (SST) data is from the National Oceanic and Atmospheric Administration (NOAA) Optimum Interpolation (OISST; Version 2) (Reynolds et al., 2002).

2.2. Global aerosol simulation

We use AOD and fAOD simulations from global aerosol models to be compared with the observations. We analyse the output from two models: the Spectral Radiation-Transport Model for Aerosol Species (SPRINTARS), and the Tracer Model 5 (TM5). In particular, we use the output from the AeroCom (Aerosol Comparisons between Observations and Models) Phase II (Schulz et al., 2009) hindcast experiment, in which the models used time-varying IPCC emissions (Lamarque et al., 2013) and reanalysis meteorology.

TM5 (Huijnen et al., 2010; Aan de Brugh et al., 2011) was driven by meteorological fields from the ERA-Interim reanalysis (Dee et al., 2011) from 2000 to 2009. The precipitation data which forced the model was also from the ERA-Interim reanalysis. As Fig. 1 shows, this precipitation data is extremely similar to the GPCP precipitation data. TM5 uses the modal microphysics scheme M7 (Vignati et al., 2004) to represent sulphate, BC, organic carbon, sea salt, dust and aerosol water, together with a thermodynamic model to describe the equilibrium of the secondary inorganics (sulphate, ammonium and nitrate). In M7, five out of the seven modes are internally mixed. The aerosol optical properties (such as AOD) are based on the Mie theory. For internally mixed aerosols, the model applies a volume-weighted mixing of refractive indices within each mode, using the well-known Bruggeman and Maxwell Garnett mixing rules (Garnett, 1904; Bruggeman, 1935), where BC and dust are treated as inclusions. The total AOD is computed by summing up the contributions from the different modes. fAOD consists of BC, OA, sulphate, nitrate and the fine-mode contributions from sea salt and dust. AOD results from the same model setup were analysed by Von Hardenberg et al. (2012).

TM5 differentiates between clear-sky and all-sky relative humidity. In calculating AOD, the clear-sky humidity is used while aerosol mass in all-sky conditions is used. Thus, the TM5 AOD can be considered clear-sky AOD overall. In comparison, satellite-derived AODs are based on clear-sky pixels while AOD in AERONET is retrieved as long as there is a gap in cloud between the sun and the instrument. In view of this, we note that TM5 AOD and MODIS + MISR + AERONET AOD have slightly different treatments of cloud effects.

Anthropogenic and biomass burning emissions were prescribed based on a combination of the Atmospheric Chemistry and Climate Model Intercomparison Project (ACCMIP) dataset for the year 2000 and the RCP4.5 scenario data for the years 2005 and 2010 (Lamarque et al., 2013), using a linear interpolation for the intermediate years. Thus, the interannual variation of the anthropogenic and biomass burning emission applied in the model is unrealistic, especially in view of no consideration of interannually-varying weather on biomass burning emission. The seasonal variation of anthropogenic emission is not realistic either, in that the ACCMIP emissions only included a seasonal variation from shipping and aircraft and ignored the seasonal variation in the other anthropogenic sectors (Lamarque et al., 2010). We find that SO_2 emission in eastern China in this emission dataset varies by less than 1% seasonally, while, as stated in section 1, SO_2 emission in China is estimated to fluctuate by 20% seasonally by Lu et al. (2011). On the other hand, the ACCMIP dataset does include the full seasonal variation of biomass burning emission. Over Africa, BC emission in the ACCMIP data is estimated to change about three-fold from the lowest emission month to the highest emission month. In comparison, the optimised BC emission estimated by Cohen and Wang (2013) gives a slightly larger seasonal fluctuation. We also note that the BC emission in the ACCMIP dataset likely has low biases; for instance, the global BC emission in the year 2000 is about 7.6 Tg while Cohen and Wang (2013)

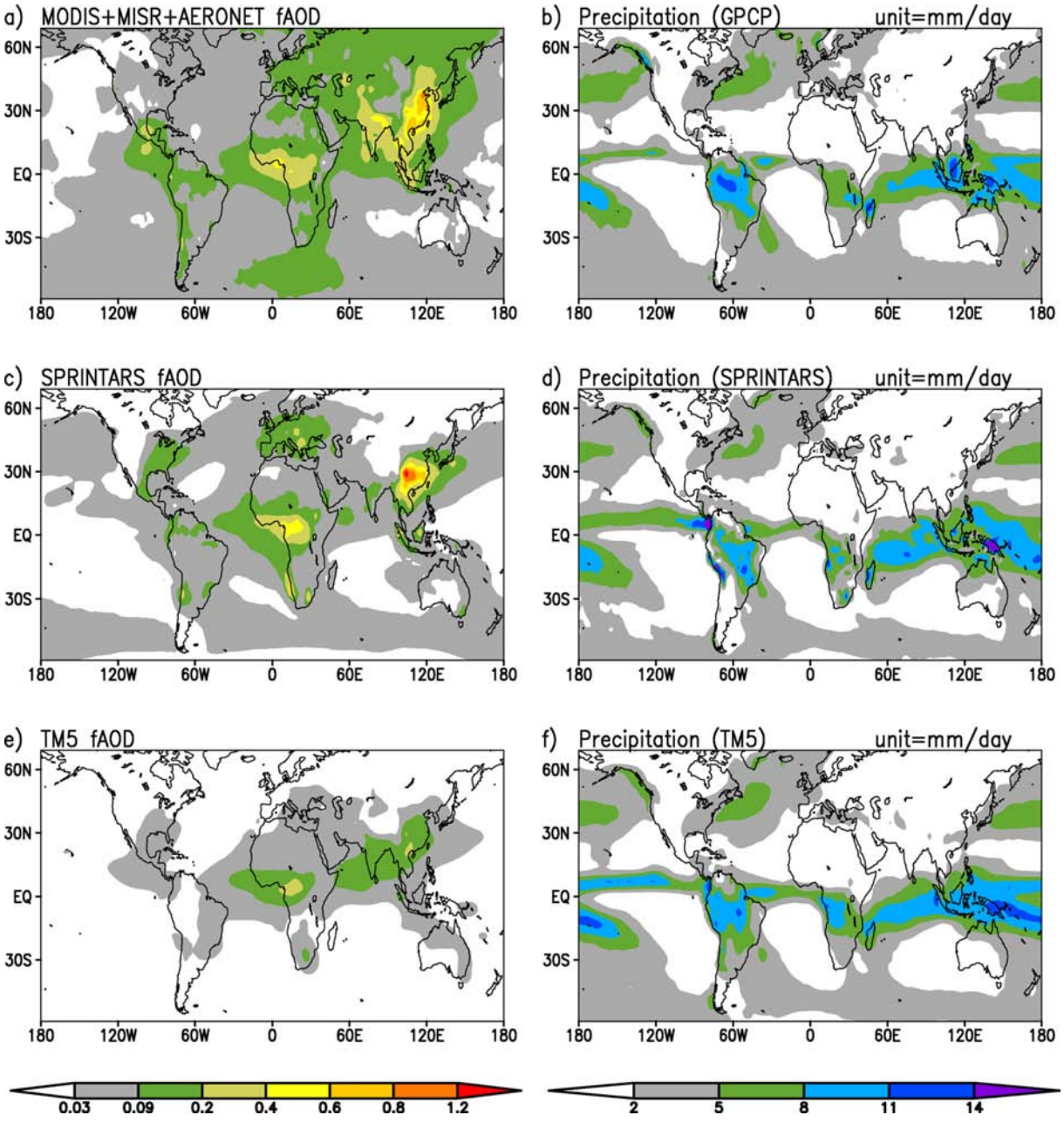

Fig. 1. 2001–2008 average fAOD (fine-mode AOD) and precipitation for the DJF (December, January, February) season.

estimate the global emission to be between 14.6 and 22.2 Tg/yr. Cohen and Wang (2013) used aerosol observations such as AERONET data to derive the estimates while Lamarque et al.'s (2010) employed a bottom-up approach. For mineral dust, the year-2000 dataset provided to AeroCom phase I as described in Dentener et al. (2006) was applied. Sea salt and dimethylsulfate (DMS) emissions were calculated online and were thus allowed to change depending on the meteorology.

The SPRINTARS is a global aerosol model (Takemura et al., 2000, 2002, 2005, 2009) coupled with a general circulation model MIROC (Watanabe et al., 2010), which includes the aerosol–radiation and aerosol–cloud interactions. The simulation in this study is nudged by temperature and horizontal wind from the National Centers for Atmospheric Prediction (NCEP)/National Center for Atmospheric Research (NCAR) reanalyses (Kalnay et al., 1996) from 1980 to 2008. In this model, aerosols are externally mixed except for BC and OA, which are mixed internally using a volume-weighted mean value for the refractive index. The total AOD is the sum of the AODs from

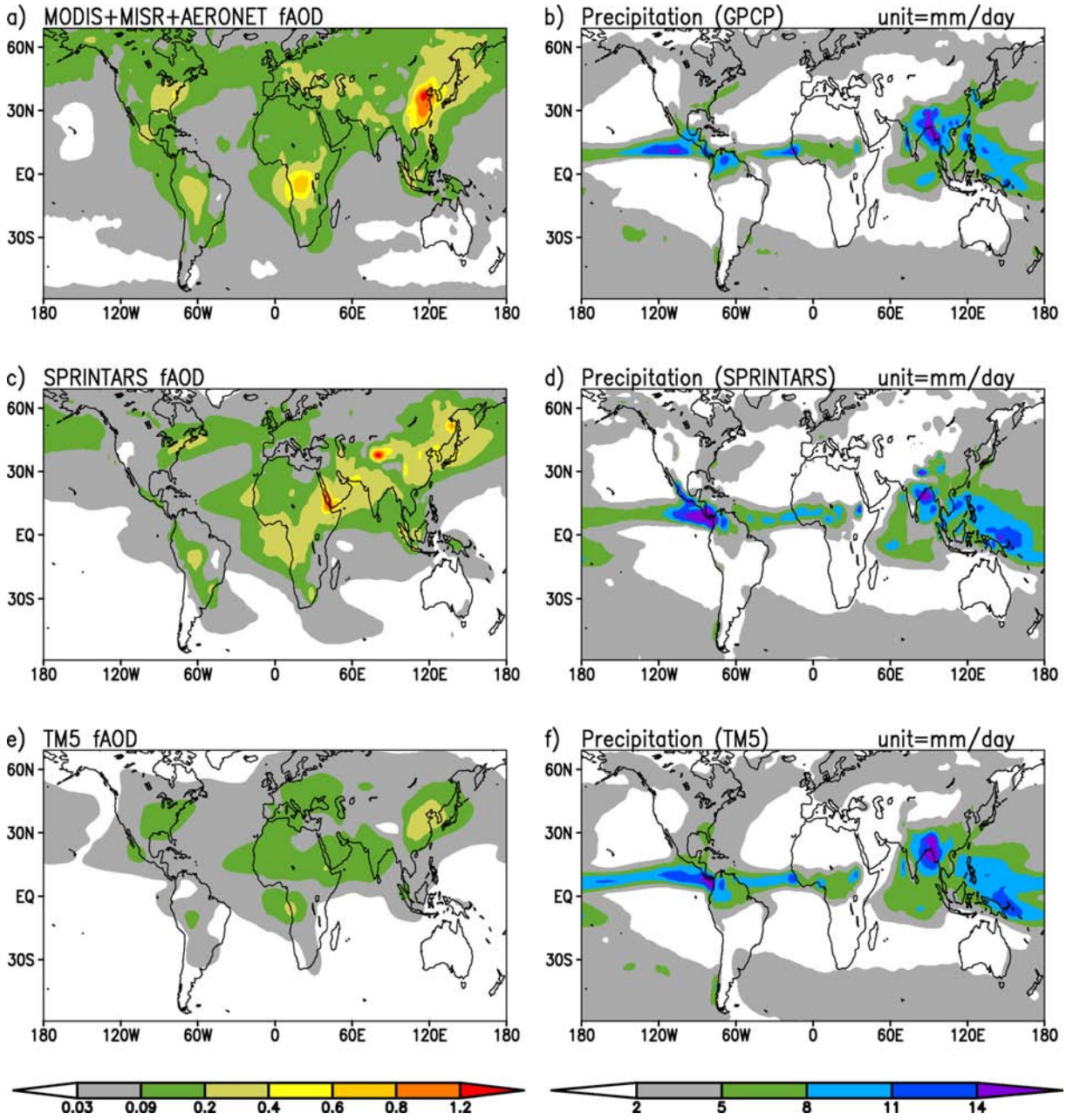

Fig. 2. Same as Fig. 1 except for the JJA (June, July, August) season.

individual aerosol species and the AOD of internally mixed BC–OA aerosol. fAOD consists of BC, OA, sulphate and the fine-mode contributions from sea salt and dust. The AOD computed in this model excludes the times and locations where the total cloud fraction is greater than 0.2, thus representing clear-sky AOD. In this regard, the treatment of cloud effect is similar to that of the observed AOD by satellite or AERONET.

Anthropogenic and biomass burning emissions are the same as in TM5. Mineral dust emission and sea salt are calculated online. The dust emissions in the SPRINTARS model are much greater than those in TM5 in Asia, whereas these two models have comparable dust emissions over the Sahara. Conversely, the sea salt emission in the SPRINTARS model is much less than that in TM5.

3. Climatology and interannual variation

Figures 1 and 2 display 2001–2008 average fAOD and precipitation for DJF (December, January, February) and

JJA (June, July, August). Among the most conspicuous features are low fAOD biases in simulations relative to the observation. SPRINTARS tends to have lower fAOD than the observation, and TM5 gives even smaller values. In a global and annual average, the MODIS + MISR + AERONET fAOD is 0.09, SPRINTARS 0.06, and TM5 0.035. Thus, the observed fAOD is 1.5 times as high as SPRINTARS fAOD and 2.6 times as high as TM5 fAOD. Simulation biases are similar for the total AOD; the MODIS + MISR + AERONET AOD is 0.161, SPRINTARS 0.089, and TM5 0.073. These low biases possibly imply that these two models have a too-fast removal of aerosols by wet deposition. It is also possible that the emission or the formation of certain aerosol types is underestimated. For example, as discussed in section 2, BC emission in the models is likely underestimated, given the observationally-constrained estimate by Cohen and Wang (2013). Another potential source of the model deficiencies is a lack of urban-scale processing in the models. Cohen et al. (2011) demonstrated that ignoring urban processing increases the global average AOD significantly. The fact that the models under-simulate AOD means that ignoring urban processing is more than offset by the factors contributing to low biases.

Another salient feature in Figs. 1 and 2 is that areas with substantial fAOD tend not to overlap with those with substantial precipitation. For instance, the biomass burning aerosols in Africa are located just north of the rainfall belt in the DJF season and south of the rainfall zone in the JJA season. The tendency for biomass burning to occur away from wet area is clearly evident in both the observation and model simulations. In contrast, the wet-area-avoiding tendency is not very clear over India and China, where fossil fuel combustion is a very important source of aerosol. In summer, the monsoon rainfall occurs over India but SPRINTARS simulates larger fAOD in summer than in winter over this region while the observation indicates otherwise. We will discuss the relationship between fAOD and precipitation in detail in the next section.

Temporal variations of fAOD can be split into the climatological seasonal variation and the deviations from the climatological seasonal variation. The latter consists largely of interannual variation and includes intraseasonal variability. For brevity, we refer to this latter as interannual variation in this study. Focusing on the climatological seasonal variation first, as the models under-simulate fAOD and AOD, the climatological seasonal variation for simulated AOD and fAOD is also suppressed. The seasonal variation relative to the annual mean however, as shown in Table 1, is not underrepresented in the models.

The spatial pattern of the climatological seasonal variation, as displayed in Fig. 3, gives additional insights. The feature that is of particular interest is the relative strength of the biomass burning aerosol variation to the fossil fuel combustion aerosol variation. We assess the relative strength by comparing the relative standard deviation (SD) of fAOD over eastern China (which represents fossil fuel combustion) to that over the Amazon and the open biomass burning areas of Africa (which together represent tropical biomass burning areas). In the observations, biomass burning fAOD has a much greater seasonal variation than fossil fuel combustion fAOD (Fig. 3b). The greater seasonal variation in biomass burning aerosol might be due partly to a greater dependence of biomass burning emission on local weather conditions. The SPRINTARS model, on the other hand, shows relatively strong seasonal variation

Table 1. Global average of SD (standard deviation)

		2001–2008 average seasonal variation RSD (%)	Interannual variation RSD (%)
AOD	MODIS alone	30.4	23.8
	MODIS + MISR + AERONET	26.3	30.0
	SPRINTARS	32.9	32.6
	TM5	23.4	15.4
fAOD	MODIS + MISR + AERONET	34.3	37.1
	SPRINTARS	38.7	37.3
	TM5	32.7	17.2
Precipitation	GPCP precipitation	46.9	49.0
	SPRINTARS precipitation	43.8	74.7
	TM5 precipitation	43.2	33.8

Note that the MODIS + MISR + AERONET data are the standard observation we use here and is from Lee and Chung (2013). To compute interannual variation SD, we use the 2001–2010 period for detrended MODIS, MISR, AERONET and GPCP data, the 1980–2008 period for detrended SPRINTARS data, and the 2000–2009 period for detrended TM5 data. In computing the global average SD, the data corresponding to the MODIS AOD gaps are removed. Instead of showing SD itself, we show the normalised values in percentage by dividing SD by mean, which is referred to as RSD (relative SD).

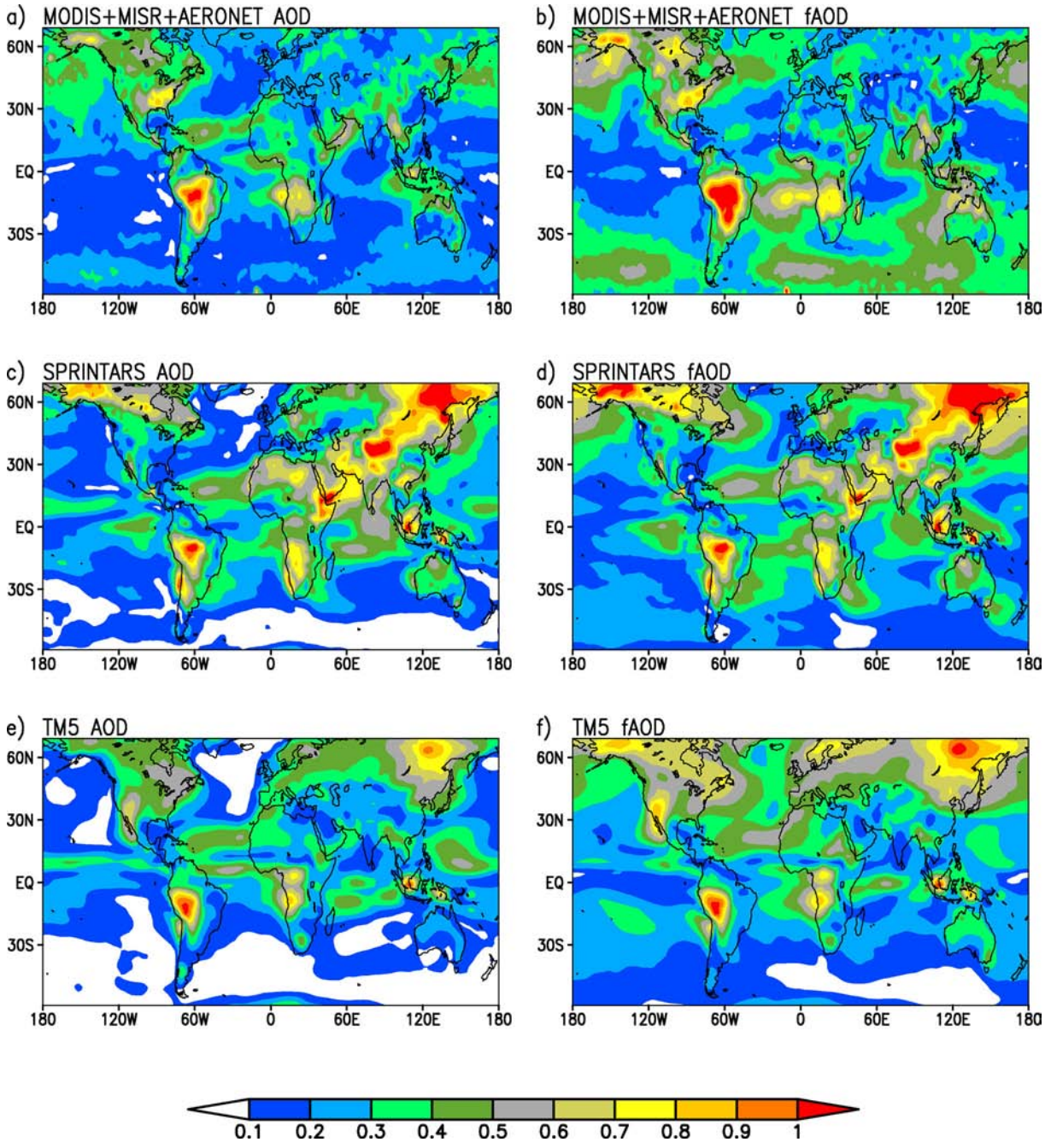

Fig. 3. RSD (Relative standard deviation) of climatological (2001–2008) seasonal variation.

over eastern China compared to the observation (Fig. 3b vs. 3d) and compared to the seasonal variation in the tropical biomass burning areas (Fig. 3d). The inconsistency between the observation and the SPRINTARS might seem counter-intuitive, in that the anthropogenic emission used by the models under-represents the seasonal variation. Lu et al. (2011) showed that SO_2 and carbonaceous aerosol emission in China is lowest in summer and highest in winter. The MODIS + MISR + AERONET fAOD is largest in summer in this region. Thus, the observation indicates that the growth of fAOD by moisture, photochemistry, etc. is sufficient to more than overcome lower emission in summer. In the models where the anthropogenic emission is not significantly lower in summer, the seasonal variation might be artificially amplified over eastern China. For TM5, however, while one might expect

to see such an artificial amplification, this model shows a weak seasonal variation in eastern China (Fig. 3f).

In a global average, the climatological seasonal variation is slightly weaker than the interannual variation in the standard AOD and fAOD observations (see Table 1). It is possible that the interannual variation is stronger than the seasonal variation because this particular observation (which combines MODIS, MISR and AERONET data) includes the AERONET data. AERONET data has an uneven coverage in time, and this uneven coverage can amplify the interannual variation component. Thus, we re-calculated the variability using the MODIS AOD and found that the climatological seasonal variation is slightly stronger than the interannual variation (Table 1). On the other hand, TM5 has most of the variability coming from the climatological seasonal variation. This is expected, because the interannual variation of the emission in the model is suppressed. Despite using the same anthropogenic and biomass burning emissions, SPRINTARS is very close to the observation in terms of the ratio of the climatological seasonal variation to the interannual variation. The difference between TM5 and SPRINTARS might be due partly to the fact that the precipitation used in TM5 also has weak interannual variation while the precipitation in SPRINTARS has very strong interannual variation (Table 1). It would be interesting to see whether the models can reproduce the observed variability partition between the climatological seasonal variation and the interannual variation with the same GPCP precipitation forcing.

The spatial pattern of the interannual variation is shown in Fig. 4. The observed fAOD interannual variation (Fig. 4b) has quite a different spatial pattern than the observed fAOD seasonal variation (Fig. 3b) does. Large interannual variation is found over the Amazon, Indonesia, Australia, Canada and some parts of remote oceans (Fig. 4b). The spatial pattern differences between the observation (Fig. 4b) and the simulations (Fig. 4d and 4f) are also very substantial. Figure 4 also reveals that the tendency for TM5 to have weak interannual variation is everywhere (Fig. 4f vs. 4d).

4. Relationship between fAOD and precipitation

Figures 1 and 2 imply that precipitation and fAOD are negatively correlated at least over tropical biomass burning areas. In this section, we investigate the correlation between precipitation and fAOD. The correlation arises from the climatological seasonal variation as well as interannual variation. Here, we compute the correlation due to the climatological seasonal variation and that due to interannual variation separately and refer to the latter as interannual correlation for brevity. The correlation due to the climatological seasonal variation is simply referred to as seasonal correlation. Interannual correlation is computed after detrending the data. Please note that our use of monthly mean clear-sky fAOD and monthly mean precipitation means that the obtained correlation does not describe an instantaneous relationship between fAOD and precipitation.

Figure 5 shows the seasonal correlation for both the observation and the models. The correlation is mostly negative over tropical biomass burning regions such as Indonesia, the Amazon and Central Africa. This feature is as expected. On the contrary, the correlation over Canada, the central part of the US and the eastern part of Siberia is positive, particularly in the models. Out of these regions, the ratio of SO_2 emission to BC emission imposed in the models is low in Canada and the eastern part of Siberia. The ratio over there is higher than over the open biomass burning regions in Africa but is comparable to that over Indonesia, which indicates that biomass burning is probably the leading aerosol source in Canada and the eastern part of Siberia. Thus, the positive correlation in these regions is a puzzle.

Figure 6 is shown to further understanding the correlation contrast between the tropical biomass burning areas and the high-latitude biomass burning areas. While fAOD seasonal variation is in antiphase with precipitation seasonal variation in Africa (Fig. 6a and 6e), the fAOD maximum in Canada occurs in summer when precipitation is neither maximum nor minimum (Fig. 6b and 6f). Figure 6 also shows the seasonal variation using AERONET data alone in order to test the robustness of MODIS + MISR + AERONET data seasonal variation. Both the AERONET data alone and the MODIS + MISR + AERONET data show the maximum fAOD in summer (Fig. 6b). Because the relationship between fAOD and precipitation over Canada is neither in phase nor in antiphase, we propose that the positive seasonal correlation over the high-latitude biomass burning areas is coincidental. We suspect that precipitation is a minor factor in controlling the fAOD over the high-latitude biomass burning areas and perhaps a greater factor is temperature. Boreal forest fires generally take place in the season when temperature is higher. In the tropics, conversely, air is always warm and thus temperature is unlikely a limiting factor. Please note that additional runs and analyses would be needed to pin down the cause for the correlation contrast, however such additional work is beyond the scope of the present study.

China is dominated by fossil fuel combustion aerosols especially in its eastern part (Chen et al., 2013). In addition, the amount of aerosol is very significant in this region which also receives a large amount of precipitation (Figs. 1 and 2). Eastern China is, in our view, a showcase for the effect of wet weather on fossil fuel combustion aerosols. The observed fAOD (Fig. 5b) shows a strongly positive

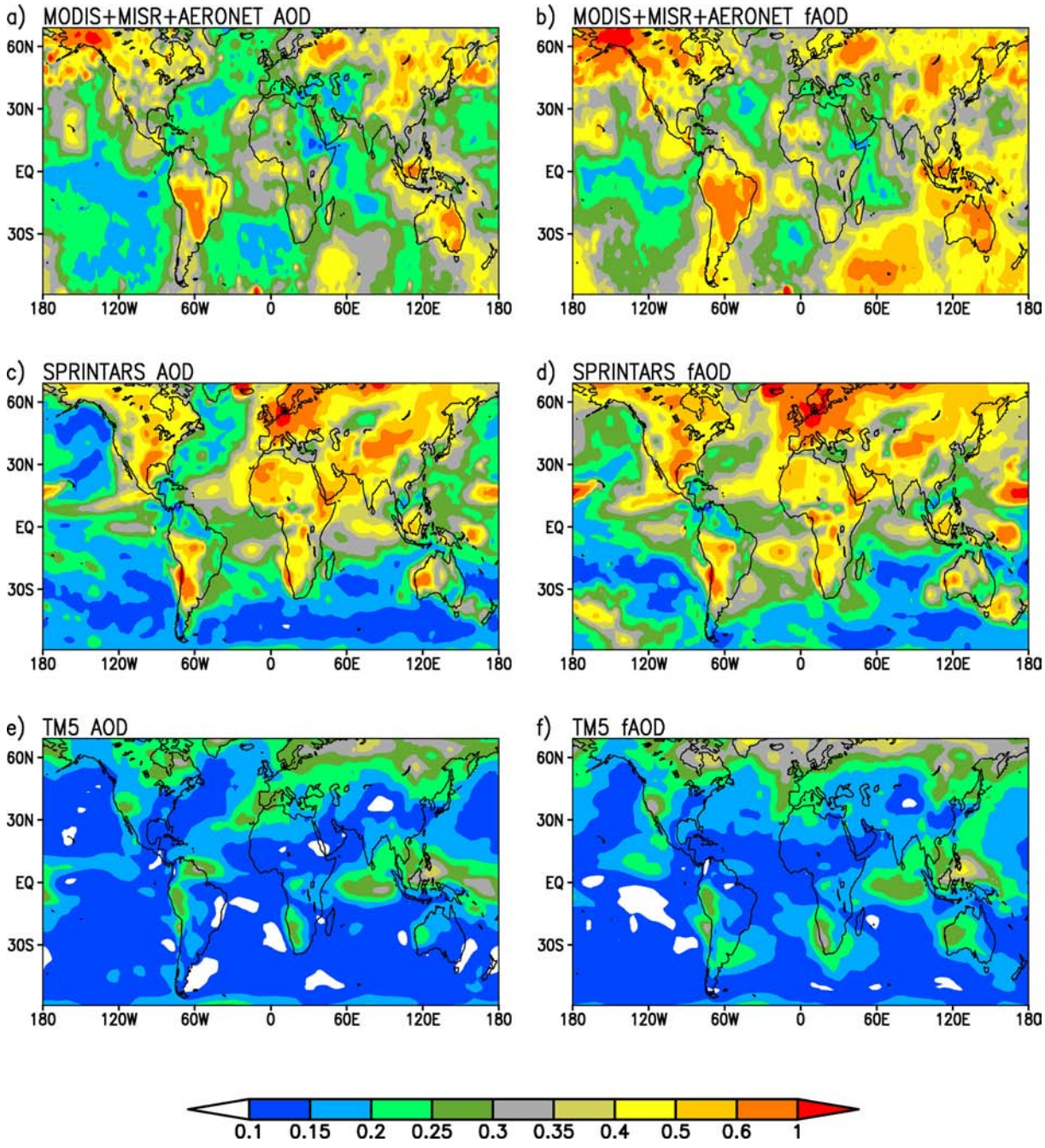

Fig. 4. RSD of interannual variation. See Table 1 for the period used for each dataset.

seasonal correlation in the eastern part of China. This is at least in part because fossil fuel combustion AOD growth (especially sulphate AOD growth) by moisture overwhelms the precipitation scavenging effect. Figure 7 shows that MODIS + MISR + AERONET fAOD and AERONET-alone fAOD are both largest in summer, when precipitation is the maximum. In terms of seasonal correlation, the simulated fAOD (Fig. 5d and 5f) agrees with the observation in the northeastern part of China but not in the southeastern part. The difference between the observation and the models in the southeastern part of China is a puzzle and would require additional model experiments for better understanding. Figure 7a demonstrates that the SPRINTARS simulates largest fAOD in spring. The fact that fAOD is neither in phase nor in antiphase with precipitation is evidence of little influence by precipitation

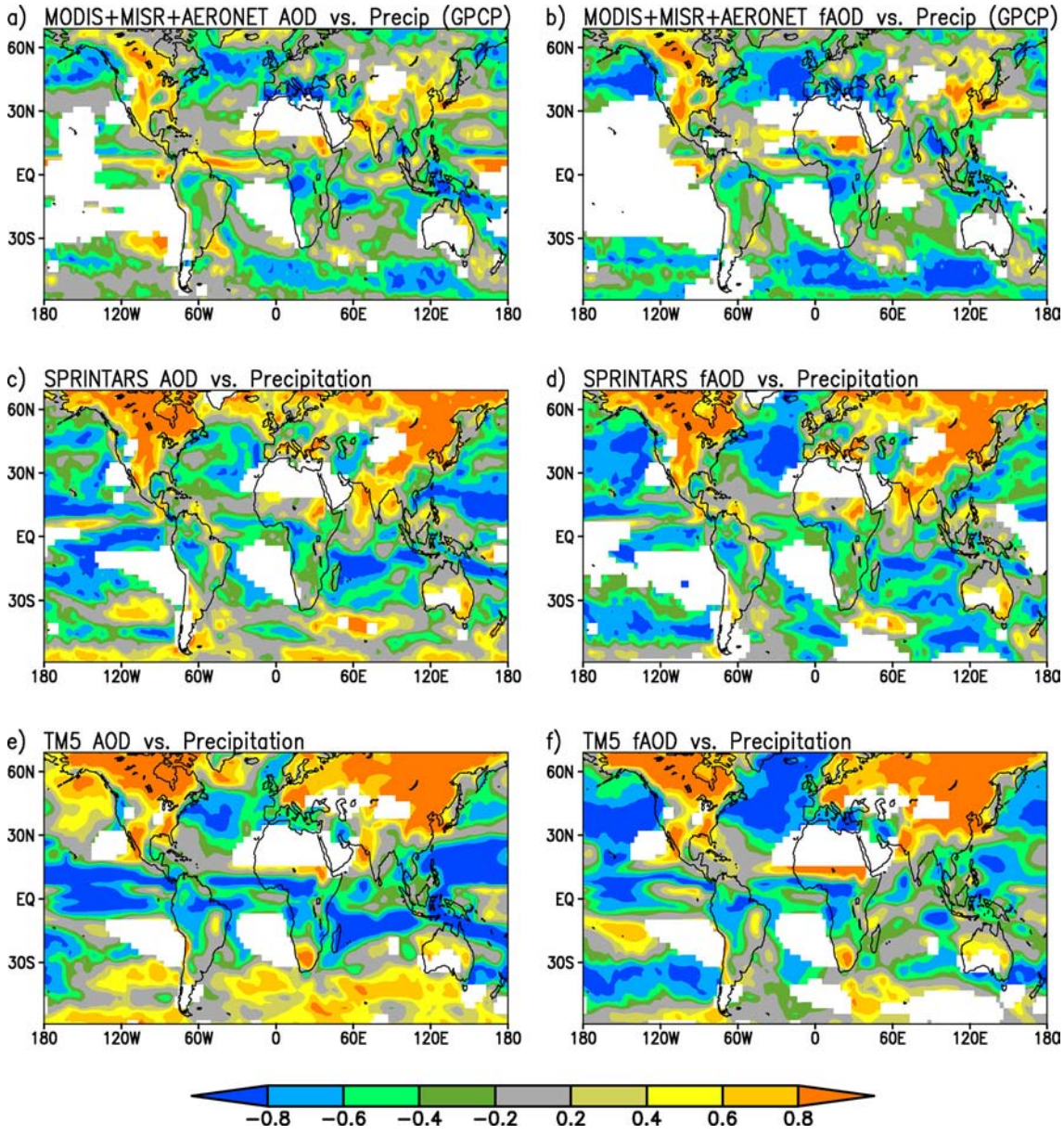

Fig. 5. Seasonal correlation between AOD (or fAOD) and precipitation. Correlation is computed using the 2001–2008 climatological seasonal variation. For consistency, precipitation used for SPRINTARS (or TM5) is used with SPRINTARS (or TM5) AOD. Regions with low AOD (or fAOD) or precipitation variance are masked out. The mask-out threshold values are: 1e-04 (MODIS + MISR + AERONET AOD), 1e-05 (SPRINTARS AOD), 1e-08 (TM5 AOD), 1e-04 (MODIS + MISR + AERONET fAOD), 1e-05 (SPRINTARS fAOD), 1e-06 (TM5 fAOD) and 0.05 (mm/day) (precipitation).

in SPRINTARS. In this regard, the negative correlation in the southeastern part of China (Fig. 5d) is not a robust feature.

India has a good mixture of fossil fuel combustion aerosols and biomass burning aerosols (Gustafsson et al., 2009). In this country, a significant fraction of biomass burning is estimated to be biofuel combustion (Bond et al., 2004), which may not depend so much on weather. In India, we see large correlation differences between AOD and fAOD, and between the observation and the models (Fig. 5). As Fig. 7 demonstrates, the observed fAOD is largest in winter, when precipitation is smallest. In contrast, TM5 shows almost season-independent fAOD, while SPRINTARS simulates largest fAOD in summer. One possible explanation for the disagreement between the models and the observation is that BC emission in the

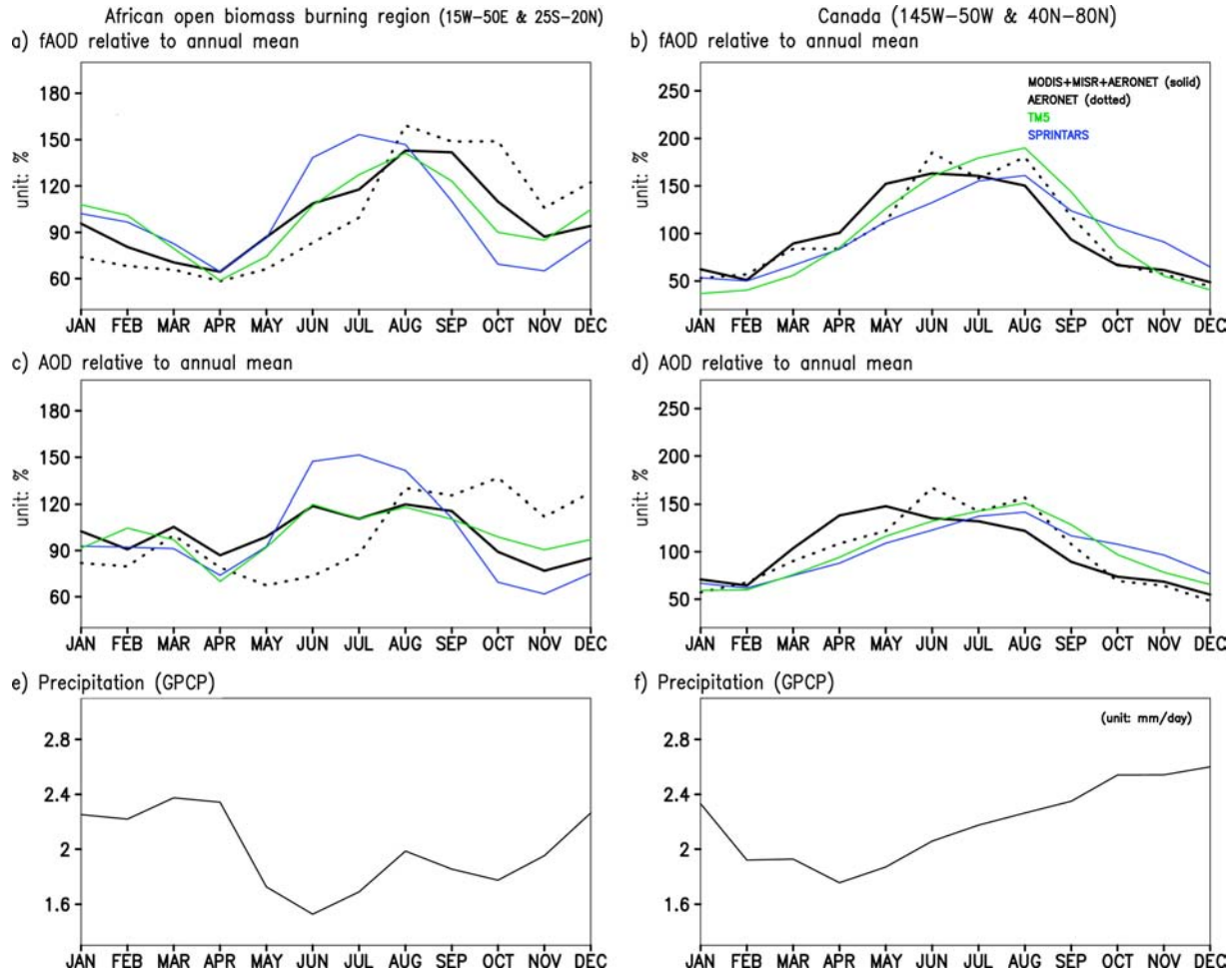

Fig. 6. 2001–2008 climatological seasonal variation of fAOD, AOD and precipitation averaged over the African open biomass burning region (defined here as 15°W–50°E & 25S°–20°N) and Canada (145°–50°W & 40°–80°N).

models is significantly underestimated in India in view of Menon et al.'s (2010) work. BC is not hydrophilic and so BC AOD will not grow by moisture unless coated by hydrophilic material. Furthermore, BC emission, which is more related to biomass burning than to fossil fuel combustion compared to SO_2 emission, is likely particularly strong in dry conditions, as demonstrated by Lu et al. (2011). Thus, it is quite possible that the observation shows a negative correlation because biomass burning aerosols dominate over India in reality while underrepresented BC emission in the models generates a relatively larger amount of sulphate and thus leads to the maximum fAOD in a moist season or seasonal independent fAOD.

The interannual variation correlation is shown in Fig. 8. The aforementioned positive seasonal correlation over the high-latitude biomass burning areas does not appear in the observed interannual variations. As shown in Fig. 8b and 8c, the correlation is more often negative than positive over these regions. Correlation with MODIS + MISR + AERONET data on interannual time scales may not be robust because AERONET data coverage changes in time. To be sure, we re-calculated the interannual correlation using MODIS AOD (Fig. 8a), which is overall consistent with the interannual correlation with MODIS + MISR + AERONET AOD. Thus, on interannual time scales, the high-latitude biomass burning aerosols also show negative correlation with precipitation. This negative correlation is statistically significant over many parts of the high-latitude biomass burning region. Thus, we conclude that wet conditions reduce biomass burning AOD over the globe. In contrast with the observations, the models simulate still (though less strong) positive interannual correlations over the high-latitude biomass burning regions. This might be because the interannual variation of emission is suppressed in the models. Additional experiments are needed to better understand the exact causes.

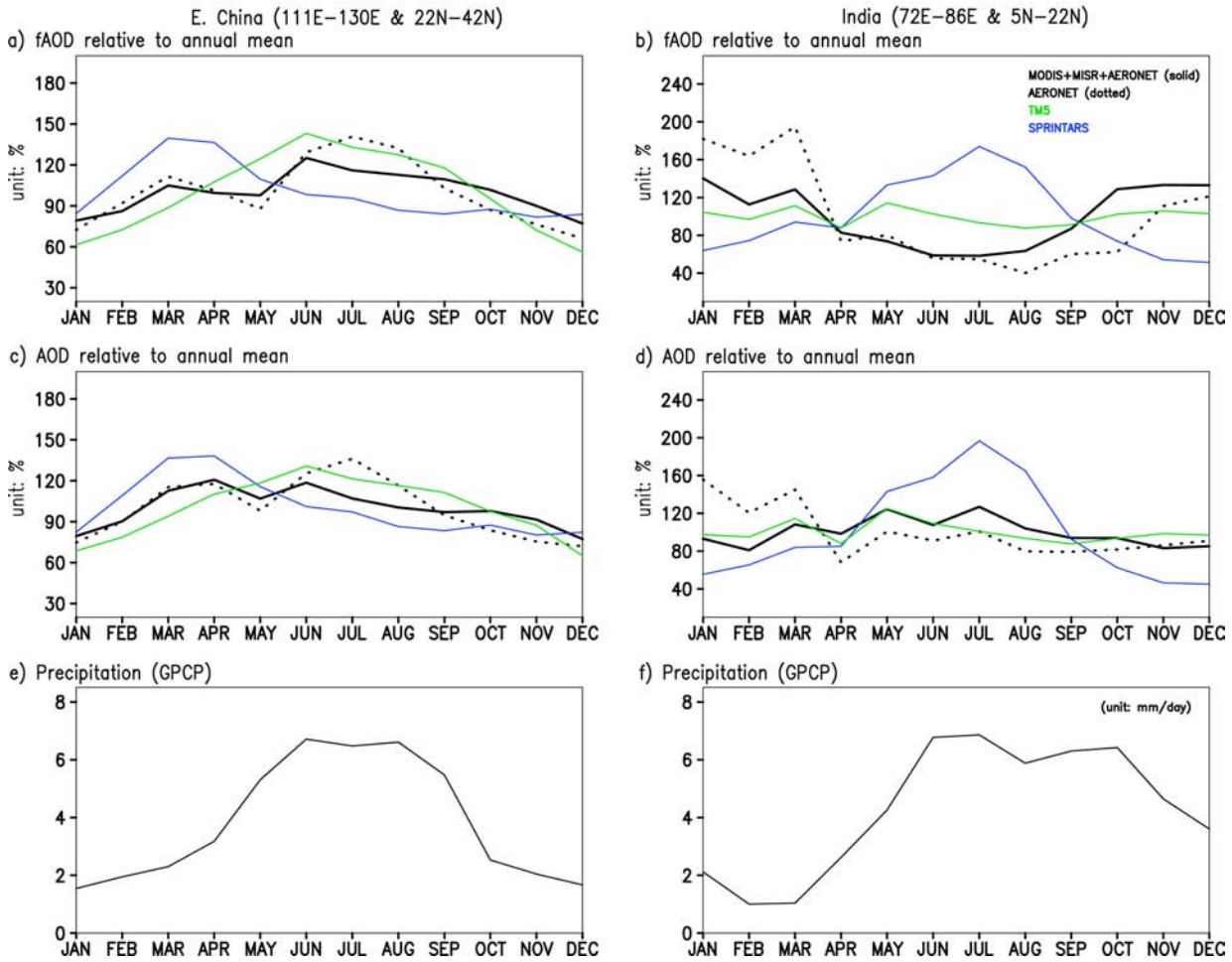

Fig. 7. 2001–2008 climatological seasonal variation of fAOD, AOD and precipitation averaged over the eastern part of China (defined here as 111°–130°E & 22°–42°N) and India (72°–86°E & 5°–22°N).

5. ENSO-covariant fAOD

To extract recurrent modes of interannual variation, such as ENSO-covariant pattern, a rotated principal component analysis (RPCA) using the VARIMAX criterion (Horel and Wallace, 1981) has been commonly applied (Nigam et al., 2000; Rogers and McHugh, 2002). At Climate Prediction Center of the US, an RPCA is routinely applied to monitor important large-scale variability modes such as North Atlantic Oscillation (NAO) and Pacific/North American (PNA) variability. In particular, a combined RPCA technique extracts recurrent patterns of combined variability by simultaneously analysing the structure of auto-covariance and cross-covariance matrices. The efficacy of this method in extracting the truly-coupled variability modes increases with the number of variables in the combination (Nigam and Shen, 1993). In view of this, we conduct an RPCA of combined interannual variation of SST, precipitation and fAOD from 2001 to 2010, from 2000 to 2008 and from 2000 to 2009 for the observation, SPRINTARS and TM5, respectively. In conducting the RPCA, 10 loading vectors are rotated.

Here, we describe the first mode which corresponds to ENSO mode, as shown in Figs. 9 and 10. To test the robustness of ENSO mode in the RPCA, we also conducted linear regression with the Nino3.4 index (which is defined as the SST anomalies averaged over the Nino3.4 region). ENSO mode obtained from the linear regression is quite similar to ENSO mode in the RPCA, which points out the robustness of ENSO mode obtained from the RPCA. As Fig. 9 shows, the positive phase (i.e. warm phase) of ENSO mode is associated with positive SST anomalies in the eastern/central equatorial Pacific, and negative SST anomalies in the central extratropical Pacific. The associated precipitation anomalies are suppression over Indonesia, South Asia, Southeast Asia and northern South America, and enhancement over the central equatorial Pacific and the central part of South America.

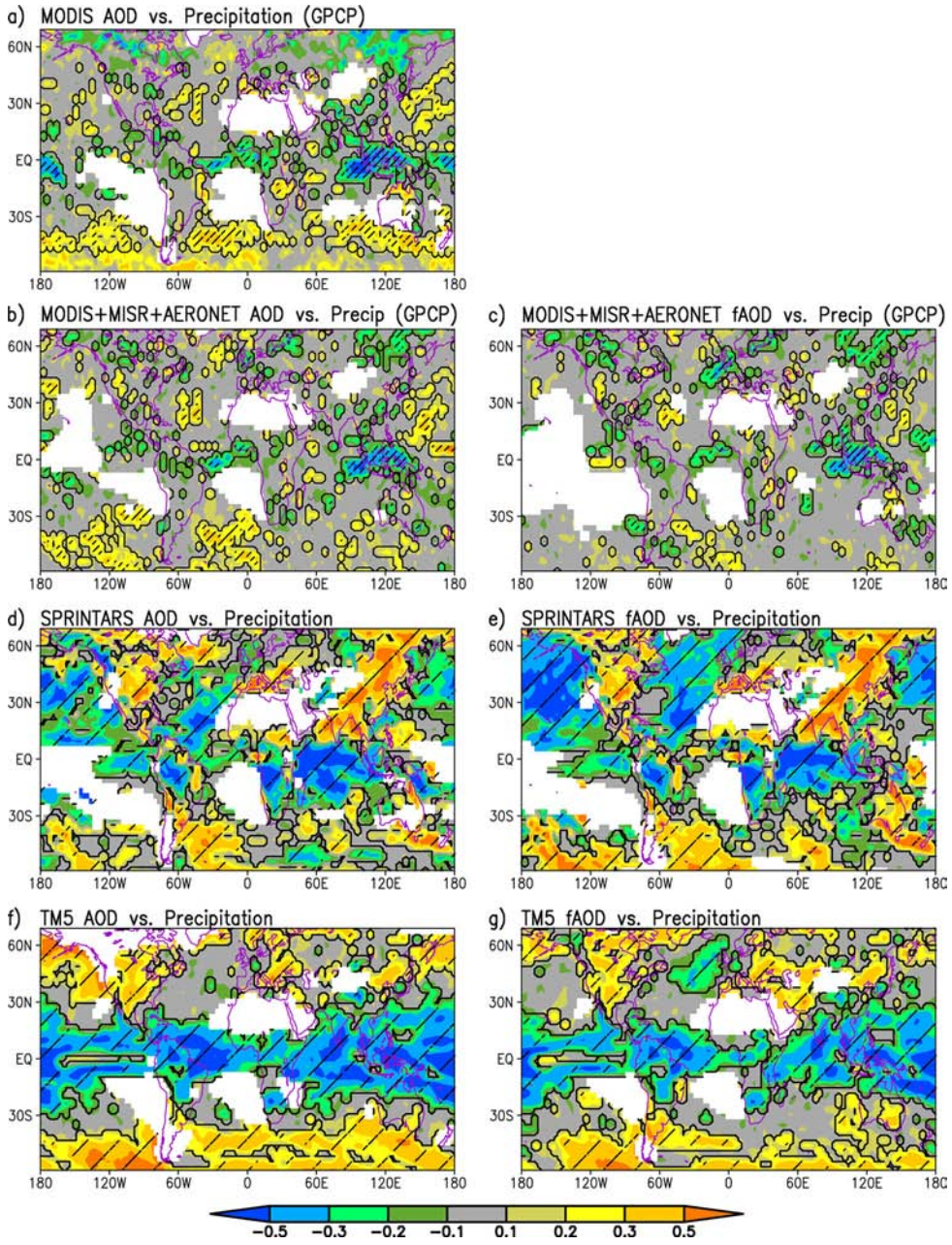

Fig. 8. Interannual correlation between AOD (or fAOD) and precipitation. Here, interannual correlation refers to the correlation with the variability other than climatological seasonal variation. Detrended data are used for the analysis. See Table 1 for the period used for each dataset. The mask-out threshold values are: 2e-04 (MODIS AOD), 2e-04 (MODIS + MISR + AERONET AOD), 5e-05 (SPRINTARS AOD), 2e-05 (TM5 AOD), 1e-04 (MODIS + MISR + AERONET fAOD), 1e-05 (SPRINTARS fAOD), 1e-06 (TM5 fAOD) and 0.05 (mm/day) (precipitation). Data corresponding to MODIS data gaps are also masked out. Correlation values in the hatched area are considered statistically significant at the 95% level, using the Effective Sample Size *t*-test.

ENSO variability is not limited to SST or precipitation. Although not shown here, ENSO also affects circulation, and so forth (see Nigam et al., 2000).

The observed ENSO-covariant fAOD is shown in Fig. 9. ENSO-covariant fAOD has large-scale features. The presence of large-scale features in ENSO-covariant fAOD attests to the robustness of ENSO impacts on fAOD. Among noticeable features is an increase over Indonesia and the eastern coastal area of China, and a decrease over South Asia, the Amazon and the continental

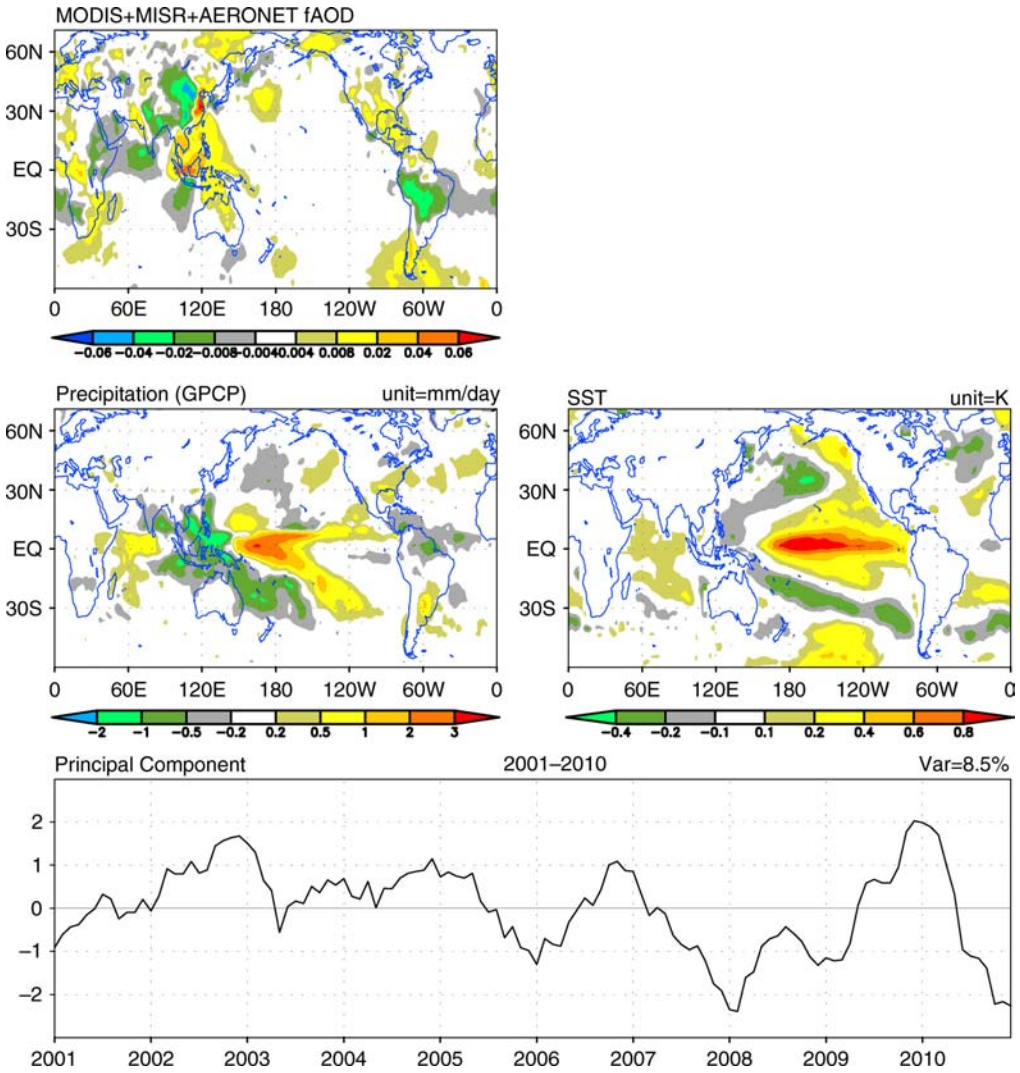

Fig. 9. Combined rotated principle component analysis (RPCA) of observed fAOD, GPCP precipitation and NOAA OI SST. Shown is the first mode.

area of China. Another aspect of the large-scale features is that these regions are teleconnected on ENSO time scales.

Figure 10 shows ENSO modes from the models. SPRINTARS and TM5 show much smaller ENSO-covariant fAOD, probably because these models (especially TM5) greatly underestimate fAOD interannual variation. These two models agree with the observation in ENSO-covariant fAOD over Indonesia. The models (especially TM5) also simulate an increase over the eastern coastal area of China. In South Asia, however, the simulations show an increase of fAOD on the contrary to the observation. In section 4, we showed that the seasonal variation of fAOD in the models is particularly deficient in India (Fig. 7). This indicates that over the area where the model performs poorly on a seasonal time scale it also performs poorly on interannual time scales.

Figure 10 also shows ENSO-covariant AOD in the observation and the models. Although ENSO AOD is generally similar in pattern to ENSO fAOD, ENSO AOD reveals additional features. For instance, over the oceanic areas south of Africa and Australia, ENSO AOD is positive in the observation (Fig. 10a). AOD in these areas likely results from sea salt aerosols. The models do not reproduce this positive AOD feature even if the models compute sea salt online. This casts doubt on the ability for the models to simulate sea salt aerosols realistically.

6. Conclusion and discussion

In this study, we have analysed combined satellite and ground observations to investigate the relationship between fAOD (and also AOD) and precipitation on seasonal and

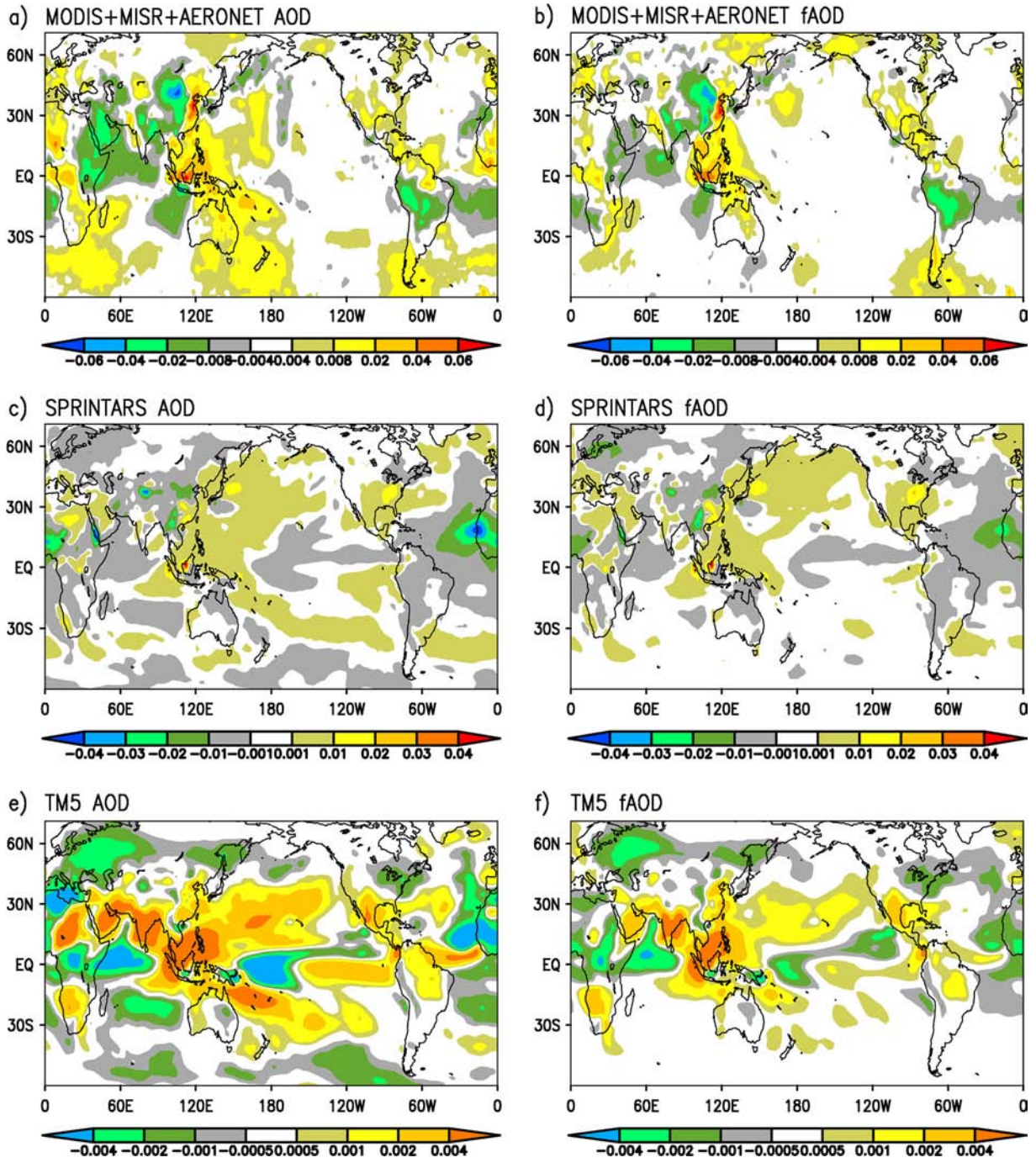

Fig. 10. ENSO mode (i.e. 1st mode) from a combined RPCA of fAOD, precipitation and SST. ENSO mode explains 7.9% of the total variance in SPRINTARS and 8.8% in TM5. AOD ENSO mode is obtained by linear regression with the 1st mode's principal component. Please note different colour schemes for different panels.

interannual time scales. By investigating the correlation for climatological seasonal variation and interannual variation separately, we have demonstrated that wet weather reduces biomass burning related fAOD and increases fossil fuel combustion related fAOD. This relationship allows ENSO impacts on fAOD to have robust large-scale features. We have also shown ENSO-covariant fAOD using an RPCA of combined interannual variation. During the warm phase of ENSO, fAOD increases over Indonesia and the eastern coastal area of China and decreases over South Asia, the

Amazon and the continental area of China. Since ENSO has been successfully predicted several months in advance (e.g. US Climate Prediction Center), one can utilise our findings to forecast fAOD over various regions of the globe.

We have also analysed the SPRINTARS and TM5 outputs from the AEROCOM Phase II hindcast experiment. These two models were driven by reanalyses. The models agree with the observations in biomass burning fAOD reduction during wet weather but only in the tropics. Furthermore, the models disagree with the observation and with each other in many other aspects. Fossil fuel combustion and biofuel combustion aerosol emissions (including aerosol precursor emissions) in the models underrepresent the seasonal variation and ignore realistic interannual variation. Even if the emission issues are factored in, some of the disagreements between the models and the observation cannot be well explained unless the model deficiencies are delineated. In particular, the models underestimate fAOD overall; cannot simulate a negative interannual correlation between biomass burning fAOD and precipitation outside of the tropics; and cannot simulate the summer-time fAOD minimum over India.

We hope that follow-up observational studies will be launched. For instance, we did not distinguish heavy precipitation from light precipitation in the analysis. Heavy and light precipitation might have very different impacts on aerosol. In order to separate heavy precipitation from light precipitation, observations on a fine time resolution would be needed. We also hope that the present study will stimulate aerosol modellers to conduct additional experiments to better understand the deficiencies. The current models need significant improvements in order to be used for reliable seasonal fAOD prediction.

7. Acknowledgements

The National Research Foundation of Korea (NRF-2013R1A2A2A01068214) supported this research.

References

Aan de Brugh, J. M. J., Schaap, M., Vignati, E., Dentener, F., Kahnert, M. and co-authors. 2011. The European aerosol budget in 2006. *Atmos. Chem. Phys.* **11**, 1117–1139.

Adler, R. F., Huffman, G. J., Chang, A., Ferraro, R., Xie, P.-P. and co-authors. 2003. The version-2 Global Precipitation Climatology Project (GPCP) monthly precipitation analysis (1979–present). *J. Hydrometeor.* **4**, 1147–1167.

Bond, T. C., Streets, D. G., Yarber, K. F., Nelson, S. M., Woo, J.-H. and co-authors. 2004. A technology-based global inventory of black and organic carbon emissions from combustion. *J. Geophys. Res.* **109**, D14203.

Bruggeman, D. A. G. 1935. Calculations of various physical constants of heterogeneous substances: part I. Dielectric constants and conductivity of mixtures of isotropic substances. *Ann. Phys. Leipzig.* **24**, 636–664.

Chen, B., Andersson, A., Lee, M., Kirillova, E. N., Xiao, Q. and co-authors. 2013. Source forensics of black carbon aerosols from China. *Environ. Sci. Technol.* **47**, 9102–9108.

Chin, M., Ginoux, P., Kinne, S., Torres, O., Holben, B. N. and co-authors. 2002. Tropospheric aerosol optical thickness from the GOCART model and comparisons with satellite and sun photometer measurements. *J. Atmos. Sci.* **59**, 461–483.

Cohen, J. B., Prinn, R. G. and Wang, C. 2011. The impact of detailed urban-scale processing on the composition, distribution, and radiative forcing of anthropogenic aerosols. *Geophys. Res. Lett.* **38**, L10808.

Cohen, J. B. and Wang, C. 2013. Estimating global black carbon emissions using a top-down Kalman Filter approach. *J. Geophys. Res. Atmos.* DOI: 10.1002/2013JD019912.

Dee, D. P., Uppala, S. M., Simmons, A. J., Berrisford, P., Poli, P. and co-authors. 2011. The ERA-interim reanalysis: configuration and performance of the data assimilation system. *Q. J. Roy. Meteorol. Soc.* **137**, 553–597.

Dentener, F., Kinne, S., Bond, T., Boucher, O., Cofala, J. and co-authors. 2006. Emissions of primary aerosol and precursor gases in the years 2000 and 1750 prescribed data-sets for AeroCom. *Atmos. Chem. Phys.* **6**, 4321.

Garnett, M. 1904. Colours in metal glasses and in metallic films. *Phil. Trans. Roy. Soc. Lond. A.* **203**, 385–420.

Gustafsson, Ö., Kruså, M., Zencak, Z., Sheesley, R. J., Granat, L. and co-authors. 2009. Brown clouds over South Asia: biomass or fossil fuel combustion? *Science.* **323**, 495–498.

Hess, M., Koepke, P. and Schult, I. 1998. Optical properties of aerosols and clouds: the software package OPAC. *Bull. Am. Meteorol. Soc.* **79**, 831–844.

Horel, J. D. and Wallace, J. M. 1981. Planetary-scale atmospheric phenomena associated with the Southern oscillation. *Mon. Weather Rev.* **109**, 813–829.

Huijnen, V., Williams, J. E., van Weele, M., van Noije, T. P. C., Krol, M. C. and co-authors. 2010. The global chemistry transport model TM5: description and evaluation of the tropospheric chemistry version 3.0. *Geosci. Model Dev. Discuss.* **3**, 1009–1087.

Jacob, D. J. and Winner, D. A. 2009. Effect of climate change on air quality. *Atmos. Environ.* **43**, 51–63.

Kalnay, E., Kanamitsu, M., Kistler, R., Collins, W., Deaven, D. and co-authors. 1996. The NCEP/NCAR 40-year reanalysis project. *Bull. Am. Meteorol. Soc.* **77**, 437–471.

Kim, J., Jung, C. H., Choi, B.-C., Oh, S.-N., Brechtel, F. J. and co-authors. 2007. Number size distribution of atmospheric aerosols during ACE-Asia dust and precipitation events. *Atmos. Environ.* **41**, 4841–4855.

Koch, D., Park, J. and Del Genio, A. 2003. Clouds and sulfate are anticorrelated: a new diagnostic for global sulfur models. *J. Geophys. Res. Atmos.* **108**, 4781.

Lamarque, J. F., Bond, T. C., Eyring, V., Granier, C., Heil, A. and co-authors. 2010. Historical (1850–2000) gridded anthropogenic and biomass burning emissions of reactive gases and

aerosols: methodology and application. *Atmos. Chem. Phys.* **10**, 7017–7039.

Lamarque, J. F., Shindell, D. T., Josse, B., Young, P. J., Cionni, I. and co-authors. 2013. The Atmospheric Chemistry and Climate Model Intercomparison Project (ACCMIP): overview and description of models, simulations and climate diagnostics. *Geosci. Model Dev.* **6**, 179–206.

Lee, K. and Chung, C. E. 2013. Observationally-constrained estimates of global fine-mode AOD. *Atmos. Chem. Phys.* **13**, 2907–2921.

Lu, Z., Zhang, Q. and Streets, D. G. 2011. Sulfur dioxide and primary carbonaceous aerosol emissions in China and India, 1996–2010. *Atmos. Chem. Phys.* **11**, 9839–9864.

Maxwell Garnett, J. C. 1904. Colours in metal glasses and in metallic films. *Philos. Trans. Roy. Soc. Lond. A.* **203**, 385–420.

Menon, S., Koch, D., Beig, G., Sahu, S., Fasullo, J. and co-authors. 2010. Black carbon aerosols and the third polar ice cap. *Atmos. Chem. Phys.* **10**, 4559–4571.

Murdiyarso, D. and Adiningsih, E. 2007. Climate anomalies, Indonesian vegetation fires and terrestrial carbon emissions. *Mitig. Adapt. Strat. Global Change.* **12**, 101–112.

Nigam, S., Chung, C. and DeWeaver, E. 2000. ENSO diabatic heating in ECMWF and NCEP–NCAR reanalyses, and NCAR CCM3 simulation. *J. Clim.* **13**, 3152–3171.

Nigam, S. and Shen, H.-S. 1993. Structure of oceanic and atmospheric low-frequency variability over the tropical Pacific and Indian Oceans. Part I: COADS observations. *J. Clim.* **6**, 657–676.

Ramanathan, V., Crutzen, P. J., Kiehl, J. T. and Rosenfeld, D. 2001. Aerosols, climate, and the hydrological cycle. *Science.* **294**, 2119–2124.

Remer, L. A., Kaufman, Y. J., Tanré, D., Mattoo, S., Chu, D. A. and co-authors. 2005. The MODIS aerosol algorithm, products, and validation. *J. Atmos. Sci.* **62**, 947–973.

Reynolds, R. W., Rayner, N. A., Smith, T. M., Stokes, D. C. and Wang, W. 2002. An improved in situ and satellite SST analysis for climate. *J. Clim.* **15**, 1609–1625.

Rogers, J. and McHugh, M. 2002. On the separability of the North Atlantic oscillation and Arctic oscillation. *Clim. Dynam.* **19**, 599–608.

Ropelewski, C. F. and Halpert, M. S. 1987. Global and regional scale precipitation patterns associated with the El Niño/Southern oscillation. *Mon. Weather Rev.* **115**, 1606–1626.

Schulz, M., Chin, M. and Kinne S. 2009. The aerosol model comparison project, AeroCom, phase II: clearing up diversity. *IGAC Newsletter*, No 41.

Schwartz, J. and Neas, L. M. 2000. Fine particles are more strongly associated than coarse particles with acute respiratory health effects in schoolchildren. *Epidemiology.* **11**, 6–10.

Tai, A. P. K., Mickley, L. J. and Jacob, D. J. 2010. Correlations between fine particulate matter (PM2.5) and meteorological variables in the United States: implications for the sensitivity of PM2.5 to climate change. *Atmos. Environ.* **44**, 3976–3984.

Takemura, T., Egashira, M., Matsuzawa, K., Ichijo, H., O'Ishi, R. and co-authors. 2009. A simulation of the global distribution and radiative forcing of soil dust aerosols at the Last Glacial Maximum. *Atmos. Chem. Phys.* **9**, 3061–3073.

Takemura, T., Nakajima, T., Dubovik, O., Holben, B. N. and Kinne, S. 2002. Single-scattering albedo and radiative forcing of various aerosol species with a global three-dimensional model. *J. Clim.* **15**, 333–352.

Takemura, T., Nozawa, T., Emori, S., Nakajima, T. Y. and Nakajima, T. 2005. Simulation of climate response to aerosol direct and indirect effects with aerosol transport-radiation model. *J. Geophys. Res. Atmos.* **110**, D02202.

Takemura, T., Okamoto, H., Maruyama, Y., Numaguti, A., Higurashi, A. and co-authors. 2000. Global three-dimensional simulation of aerosol optical thickness distribution of various origins. *J. Geophys. Res. Atmos.* **105**, 17853–17873.

Van der Werf, G. R., Randerson, J. T., Giglio, L., Collatz, G. J., Kasibhatla, P. S. and co-authors. 2006. Interannual variation in global biomass burning emissions from 1997 to 2004. *Atmos. Chem. Phys.* **6**, 3423–3441.

Vignati, E., Wilson, J. and Stier, P. 2004. M7: an efficient size-resolved aerosol microphysics module for large-scale aerosol transport models. *J. Geophys. Res. Atmos.* **109**, D22202.

Viskari, T., Asmi, E., Virkkula, A., Kolmonen, P., Petäjä, T. and co-authors. 2012. Estimation of aerosol particle number distribution with Kalman Filtering – part 2: simultaneous use of DMPS, APS and nephelometer measurements. *Atmos. Chem. Phys.* **12**, 11781–11793.

Von Hardenberg, J., Vozella, L., Tomasi, C., Vitale, V., Lupi, A. and co-authors. 2012. Aerosol optical depth over the Arctic: a comparison of ECHAM-HAM and TM5 with ground-based, satellite and reanalysis data. *Atmos. Chem. Phys.* **12**, 6953–6967.

Watanabe, M., Suzuki, T., O'ishi, R., Komuro, Y., Watanabe, S. and co-authors. 2010. Improved climate simulation by MIROC5: mean states, variability, and climate sensitivity. *J. Clim.* **23**, 6312–6335.

Wise, E. K. and Comrie, A. C. 2005. Meteorologically adjusted urban air quality trends in the Southwestern United States. *Atmos. Environ.* **39**, 2969–2980.

Wu, R., Wen, Z. and He, Z. 2013. ENSO contribution to aerosol variations over the maritime continent and the Western North Pacific during 2000–10. *J. Clim.* **26**, 6541–6560.